IPFx: Extended integrated particle filter method for achieving high-performance earthquake early warning system

Masumi Yamada[1], Koji Tamaribuchi[2], Stephen Wu[3]

Key Points:

1) False alarms due to source estimation errors occur in the current earthquake early warning system in Japan.

2) This method improves detection sensitivity of the current system and enables faster and more accurate warnings.

3) This method offers the potential of expanding the successful Japanese EEW method to global seismic networks.

Declaration of Competing Interests:

The authors acknowledge there are no conflicts of interest recorded.

M. Yamada, Disaster Prevention Research Institute, Kyoto University, Uji, Gokasho, 611-0011, Japan

Abstract. An earthquake early warning (EEW) system rapidly analyzes seismic data to report the occurrence of an earthquake before strong shaking is felt at a site. In Japan, the integrated particle filter (IPF) method, a new source estimation algorithm, was recently incorporated into the EEW system to improve the source estimation accuracy during active seismicity. The problem of the current IPF method is that it uses the trigger information computed at each station in a specific format as the input and is therefore applicable to only limited seismic networks. This study proposes the extended IPF (IPFx) method to deal with continuous waveforms and merge all Japanese real-time seismic networks into a single framework. The new source determination algorithm processes seismic waveforms in two stages. The first stage (single-station processing) extracts trigger and amplitude information from continuous waveforms. The second stage (network processing) accumulates information from multiple stations and estimates the location and magnitude of ongoing earthquakes based on Bayesian inference. In 10 months of continuous online experiments, the IPFx method showed good performance in detecting earthquakes with maximum seismic intensity $\geq$3 in the Japan Meteorological Agency (JMA) catalog. By merging multiple seismic networks into a single EEW system, the warning time of the current EEW system can be improved further. The IPFx method provides accurate shaking estimation even at the beginning of event detection and achieves seismic intensity error $<$0.2 5 s after detecting an event. This method correctly avoided two major false alarms on January 5, 2018, and July 30, 2020. The IPFx method offers the potential of expanding the JMA IPF method to global seismic networks.

Introduction

An earthquake early warning (EEW) system rapidly analyzes seismic data to detect the occurrence of an earthquake as soon as possible, before strong shaking is felt at a distant site. In Japan, the Japan Meteorological Agency (JMA) provides the warnings to the public. The JMA uses two different approaches for estimating the seismic intensity: a source-determination approach and a wave propagation approach. The former uses the integrated particle filter (IPF) method [Liu and Yamada, 2014; Tamaribuchi et al., 2014; Wu et al., 2014] along with the conventional not-yet-arrived method Horiuchi et al. [2005] and Hypoon method [Hamada, 1983; Ueno et al., 2002]. The latter uses the propagation of local undamped motion (PLUM) method [Hoshiba, 2013; Hoshiba and Aoki, 2015; Kodera et al., 2018]. The IPF and PLUM methods were, respectively, incorporated into the EEW system in December 2016 and March 2018, and as a result, the accuracy of shaking estimation has been improved greatly [Kodera et al., 2020].

The IPF method is a novel source determination algorithm that was developed after the 2011 Tohoku earthquake [Liu and Yamada, 2014; Tamaribuchi et al., 2014; Wu et al., 2014]. One of the unique features of the IPF method is its smart phase association process. When a new trigger is received, it is classified into either an existing earthquake or a new earthquake based on the P-wave arrival time and amplitude. The trigger information (P-wave arrival time and waveform amplitude) classified as an ongoing earthquake is used for source estimation. The waveform amplitude constrains the location at the beginning of the rupture since the difference between the P-wave amplitude and noise level is significant.

The current IPF method is designed to operate under the JMA seismic observation system. The JMA seismic observation system (including the JMA strong motion stations, DONET, KiK-net, and S-net (Seafloor observation network for earthquakes and tsunamis along the Japan Trench)) will send trigger information when a station detects seismic waves using strong motion seismometers. The IPF method uses trigger information sent by these systems but not Hi-net (High-Sensitivity Seismograph Network), another dense seismic network in Japan, because its sensor type and trigger system are different.

This study aims to extend the IPF method to continuous waveforms and merge all Japanese real-time seismic networks into a single framework. Although the IPF method improves the source estimation accuracy, the JMA EEW has sometimes published false alarms. For example, an EEW was issued for an earthquake near Torishima Island in July 2020 with an estimated JMA seismic intensity scale 5 upper (hereafter called simply "seismic intensity"). However, no station recorded a seismic intensity of 1 or larger. This false alarm was caused by an incorrect epicenter location estimate (more than 400 km away) and, in turn, an overestimated magnitude. The IPF method could not provide a reliable estimation owing to an insufficient station density, and other methods mislocated this event. Such false alarms could be avoided by merging all seismic networks and increasing the station density for the IPF method.

Data

We used continuous seismic data recorded using Hi-net and S-net from January 1 to October 31, 2020 (see Data and Resources section) for the online experiment. Hi-net has around 800 stations with a 3-component short-period velocity sensor on mainland Japan. S-net has around 150 stations with multiple sensors at the ocean bottom off the Tohoku region. We used the S-net acceleration sensors. No seismic station of these networks is present on Japan's southern island; therefore, we selected earthquakes occurring north of 30°N for the performance evaluation.

These real-time data are provided by JDXnet under a seismic data distribution agreement [Urabe et al., 2013]. The waveform data are received as 1 s User Datagram Protocol

(UDP) packets at the server in our institute, and the data are stored in the shared memory. We use a program in the Win system (a set of programs that is widely used in Japan to process seismic data) [Urabe, 1991] to read the data every second and write to the standard output. Notably, JMA strong motion data are not provided online and were, therefore, not used in our analysis.

The public is warned if the maximum estimated JMA seismic intensity is ≥5 lower. An EEW forecast is provided to specific users for lower intensities: maximum estimated seismic intensity ≥3 or estimated JMA magnitude (hereafter called simply "magnitude") ≥3.5. The event detection process commences from a single trigger, but at least two stations are required for public warning. In the 10-month test period, 129 earthquakes had maximum seismic intensity ≥3; these were used for the performance evaluation in this study.

We used three earthquakes for comparison with the JMA EEW: a successful warning by the JMA on June 25, 2020, off the Ibaraki prefecture; a false alarm on July 30, 2020, near Torishima island; and a false alarm on January 5, 2018, off the Ibaraki prefecture.

In this study, we define a false alarm as an EEW that estimates seismic intensity ≥5 lower although the observed seismic intensity is ≤3. This corresponds to a situation in which public warning is provided but the shaking is relatively minor. An accurate estimate is defined as an EEW for which the difference between the maximum observed and estimated seismic intensity (i.e., seismic intensity error) is ≤1. Further, an inaccurate estimate is defined as an EEW with a seismic intensity error >1.

IPFx Method

The extended IPF (IPFx) method is a two-step source determination algorithm. First, a single-station processing step is performed, and then, the network processing step from the original IPF method is performed. In addition, the original structure of the IPF algorithm for multievent detection is refined to make it more robust to noise. The single-station processing step focuses on the extraction of station trigger and amplitude information from continuous waveforms that are accumulated into a single data package for source estimation in the network processing step based on Bayesian inference [Wu et al., 2014].

One of the major differences between the original IPF and IPFx methods is the single-station processing step. The IPFx method uses continuous waveforms and a centralized process, whereas the original IPF method computes the trigger information at each station. The advantage of the centralized system is that we can include data from other seismic networks easily and modify the trigger conditions without updating information from each station. Using this advantage, we tuned the trigger threshold. Compared to the current IPF system, the triggering threshold is lowered in the IPFx method to avoid missing the key trigger at the station closest to the earthquake. This may increase the risk of false alarms due to noise if a warning is issued on the basis of a single station. As a tradeoff, multiple triggers (three triggers for mainland stations and two triggers for island stations) or a very large amplitude (acceleration of 100 Gal) are required for source estimation to avoid creating too many EQ processes.

Events detected using the IPFx method are categorized as pending earthquakes (EQp), ongoing earthquakes (EQ), or converged earthquakes (EQc). Each category represents a different level of confidence for an event identified by the system. Considering the tradeoff among the source estimation accuracy, computational burden, and potential station noise, predefined station groups are assigned to each category as the source of the most relevant data used for updating estimations of an event. Each component in the IPFx method is described below.

STEP 1: Single-station Processing

Our server receives continuous seismic data every second as a 1 s UDP packet, and the data are passed to the single-station processing as a standard input. A picking program processes these continuous data and extracts trigger information (P-wave arrival time and amplitudes) every second. This process is applied to each station separately and does not require communication between stations. Seismic waveforms are processed by first removing the DC offset and correcting the instrumental response [Zhu, 2003; Yamada et al., 2014]. Then, this waveform is used for P-wave detection, amplitude computation, and teleseismic filtering. The obtained information is transmitted to the network processing scheme every second as a packet.

For P-wave detection, a second-order one-pass band-pass filter with a corner frequency of 5–10 Hz is used to suppress the low-frequency noise after large earthquakes as well as high-frequency environmental noise. Phase arrivals are detected using the T^{pd} method [Hildyard et al., 2008; Hildyard and Rietbrock, 2010]. This method is computationally inexpensive and is less affected by noise than the conventional short-term average (STA)/long-term average (LTA) method [Allen, 1978].

The waveforms are integrated or differentiated, and a set of the maximum acceleration, velocity, and displacement (vector sum of three components) is computed every second. These amplitudes are used for the magnitude computation depending on the magnitude estimation equation. The JMA magnitude uses velocity and displacement components. The maximum vertical velocity is also computed for source estimation.

The teleseismic filter is a linear filter used to discriminate the possible teleseismic events from local earthquakes [Kuyuk et al., 2014; Chung et al., 2019]. The amplitudes of the vertical velocity record bandpass-filtered at 0.375–0.75 Hz and 6–12 Hz are used. The teleseismic flag is on if the amplitude of the 0.375–0.75 Hz component is larger than that of the 6–12 Hz component.

In addition to this picking information, each packet contains the station code, station status (alive or dead), packet loss, data recording time (timestamp), and data receiving time at server.

STEP 2: Network Processing

Earthquake Detection

The picking information is transmitted to the network for processing, and the next process estimates the location and magnitude of the ongoing earthquake. To prevent false alarms owing to noise contamination, multiple triggers in a small area are required to confirm earthquake detection. This station group is called a trigger group. In the proposed system, a new trigger that does not correspond to any existing events is categorized as a pending earthquake (EQp), defined as a potential event that has not yet been confirmed as a real earthquake. If enough triggers are recorded in the corresponding trigger group, an earthquake is considered detected and the source estimation process starts (see Figure 1).

Pending Earthquake (EQp): A new EQp is created with a triggered station that does not belong to any of the existing events recorded in the system (Figure 1 S4-A1). If enough triggers are recorded in the corresponding trigger group (in this case, three triggers for mainland stations and two triggers for island stations) or a very large amplitude is observed (acceleration of 100 Gal), an event is detected and the source estimation process starts (i.e., EQp is changed into EQ, Figure 1 S3-A2). Otherwise, the EQp expires and is deleted after a theoretical time frame denoted by the "virtual P-wave" passing the most distant station in the trigger group (Figure 1 S1-A5).

Trigger Group: The trigger group of one station includes all stations within 30 km (red triangles in Figure 2(a)) and the stations in the neighboring Voronoi cells within 50 km (blue triangles in Figure 2(a)). If the total number of stations is less than five, the next closest stations up to five stations are added to this group (black triangles in Figure 2(a)). The number of trigger groups varies depending on the station density. These distances are adjusted for the Japanese seismic network such that at least five stations are included in a trigger group.

Source Estimation

The detected earthquake, denoted as an EQ, is analyzed in the source estimation process. The source parameters of the EQ are continuously updated using real-time data from the seismic network (Figure 1 S1-A1). To reduce the computation time, a limited number of stations, called an estimation group, is used for source estimation.

Ongoing Earthquake (EQ): The source parameter estimates for the EQ are updated every second until the event meets any condition for cancellation (Figure 1 S1-A2) or becomes a converged earthquake (Figure 1 S1-A3). The source parameters are estimated using the IPF method [Tamaribuchi et al., 2014; Wu et al., 2014]. Particles are distributed in a three-dimensional parameter space (latitude, longitude, and depth). The likelihood of each particle is defined as a function of the P-wave arrival time and amplitude. Here, the maximum vertical velocity up to 5 s after the P-wave onset is used as an amplitude. We expect the effects of the S-wave to be small since we use the vertical component. Particles are resampled if the optimal location estimate is far from the center of the particles. The magnitude is computed from the estimated source locations and the amplitude of the waveforms [Liu and Yamada, 2014; Tamaribuchi et al., 2014; Wu et al., 2014]. An EEW is issued if the estimated seismic intensity of the EQ exceeds the warning threshold. For the earlier intervals with number of triggers less than three, the depth is fixed at 10 km.

If there is only one trigger, we fix the location at the first trigger station. This will avoid overestimating the magnitude and providing uncertain alarms over a wide region. If two or three triggers are available, we perform source estimation based on the prior particle distribution (less than 100 km from the first trigger station).

Estimation Group: An estimation group is a set of stations used for source estimation. It includes the closest 20 stations from the first trigger station (red triangles in Figure 2(b)) and another set of the closest 20 stations from the center of the Voronoi cell of the first trigger station (blue triangles in Figure 2(b)). These stations should be less than 200 km from the first trigger station. Another 10 stations are selected to improve the azimuthal coverage from the center of the Voronoi cell (black triangles in Figure 2(b)). These numbers are chosen empirically to balance the tradeoff between the P-wave travel time and the azimuthal coverage. The selection of the estimation group will need to be tuned for future application to different networks.

Convergence of Source Estimation

If the estimated source parameters converge, the source estimation process is terminated and the EQ is converted into a converged earthquake (EQc). The EQc phase is designed to reduce the computation burden of the system in handling multiple source estimation processes.

Converged Earthquake (EQc): An EQc is an event that has a stable source estimate and that may yet cause new station triggers. The EQ is converted into an EQc if the source estimate is stable for 5 s continuously after the maximum theoretical P-wave arrival time for the stations in the estimation group. The minimum convergence time (i.e., the EQ will not converge in at least this period) for EQ is empirically set to 30 s for $M<5$, 50 s for $5\leq M<6$, 70 s for $6\leq M<7$, and 100 s otherwise. The convergence time was determined such that all stations in the estimation group recorded maximum amplitudes. The EQc is deleted from the system after a predefined time threshold with no P-wave detection in the entire network, which signifies the end of a seismic sequence. This threshold for EQc is empirically set to 300 s for M<3, 600 s for 3≤M<6, and 900 s otherwise.

Cancellation of source estimation

Although multiple triggers or a single trigger of large amplitude are required to detect an earthquake, an event may be caused by multiple noises or a very small earthquake that triggers only a few stations. The EQ is removed from the source estimation process when the seismic data is no longer consistent with the source estimates (i.e., more than half the stations in the cancellation group have an error $>4\sigma$ from the estimated arrival time and the observed seismic intensity is <5 lower, Figure 1 S1-A2). This cancellation process is added to avoid recording small uncertain earthquakes in the seismic catalog. Although these events are removed from the catalog, an EEW is issued if the estimated seismic intensity exceeds the threshold before removal.

Cancellation Group: A cancellation group is a subset of the estimation group used for deleting the source estimation process. The closest 20 stations from the first trigger station are used as the cancellation group (red triangles in Figure 2(b)).

Teleseismic earthquakes

Teleseismic earthquakes could trigger inland stations depending on their travel path and the local site conditions. Estimating the location of such earthquakes is difficult because the incident angle of the waveforms is almost vertical and the apparent velocity is large. Although the shaking intensity of teleseismic earthquakes is very small, these earthquakes sometimes record relatively large magnitude owing to their large long-period component. To avoid a false alarm in response to teleseismic earthquakes, we do not issue an EEW if events satisfy the following conditions: the ratio of teleseismic flags in the total triggers in the cancellation group is >0.9 and the observed seismic intensity is <0. The second condition is necessary because some near-field deep earthquakes produce a long-period ground motion that turns the teleseismic flag on.

Results

The proposed IPFx method detected 26261 converged earthquakes during the 10-month test period. Its performance was compared with that of the JMA unified earthquake catalog (hereafter called "JMA manual catalog") and JMA EEW for relatively large earthquakes (with observed seismic intensity $\geq$3).

Comparison with Manual Catalog

Figures 3 and 4 show the accuracy of the IPFx catalog for 129 earthquakes with observed seismic intensity $\geq$3. As a result, 95% of earthquakes had a location error $\leq$10 km, magnitude error $\leq$0.59, and seismic intensity error $\leq$1. The location error tends to be larger for offshore earthquakes.

We define an accurate estimate as an EEW for which the seismic intensity error is $\leq$1. Accordingly, the estimates for all 129 earthquakes are accurate. The performance of the shaking estimation for the target earthquakes was found to be reasonably good.

The source estimation accuracy during the initial period with limited triggers plays an important role in the EEW. Figure 5 shows a time history of the errors of source parameters for 129 earthquakes with a maximum observed seismic intensity $\geq$3. The location error tends to be large right after the detection of an earthquake, and it decreases as a function of time. The average location error of inland earthquakes is initially $\sim$6 km, and it converges to 2 km 10 s after event detection. The location error for offshore earthquakes is around three times larger than that for inland earthquakes, and the convergence time is longer ($\sim$20 s). By contrast, the convergence time of the seismic intensity is similar for both offshore and inland earthquakes. The seismic intensity is initially underestimated by 1.0–1.5, and the error is less than 0.2 at 5 s after event detection. Because an EEW is issued based on the seismic intensity, a smaller initial error is very advantageous from the viewpoint of how rapidly the warning is conveyed. The difference in seismic intensity errors between offshore and inland earthquakes is very small despite the larger location error of offshore earthquakes.

Figure 6 shows a histogram of the magnitude of the JMA manual catalog and IPFx automatic catalog for all 26261 events. The IPFx method detected most earthquakes with a magnitude >3. The IPFx catalog uses the velocity magnitude (Mv) for small earthquakes and the displacement magnitude (Md) for Mv >4. Therefore, a discontinuity occurs at M = 4 owing to the difference in the definition between Mv and Md.

Comparison with JMA EEW

We compared the performance of the IPFx method with that of the JMA EEW method. Figure 7 shows the time of the first P-wave detection and the first EEW report (event detection) for both methods. The time of the first P-wave detection depends on the network density. Because the IPFx method uses multiple networks, P-wave detection is much faster than in the JMA EEW method, except for several earthquakes that occurred on islands farther from the Japanese mainland where only JMA strong motion stations were present. The time of the first EEW report was significantly improved because the IPFx method reports the first result if three stations are triggered, whereas the JMA EEW method waits until at least 3 s after the first P-wave detection. This figure shows the possibility of faster EEW with the IPFx method.

Figure 3 shows the accuracy of the JMA EEW final reports for earthquakes with observed seismic intensity ≥3. Notably, the JMA EEW method detected 111 earthquakes; 18 earthquakes were missed. Because the JMA EEW announces earthquake locations with only one decimal place, the location error does not have a good resolution. The IPFx method achieves similar source estimation accuracy to the JMA EEW method.

The IPFx and JMA EEW methods were compared in detail for three significant earthquakes: the June 25, 2020, earthquake off Ibaraki prefecture (M6.1) with a successful warning by the JMA and two false alarms on July 30, 2020, and January 5, 2018.

Figure 8 shows the result of the earthquake that occurred at 4:47:44 on June 25, 2020, off Ibaraki prefecture. The observed seismic intensity was 5 lower, and the JMA provided an appropriate warning. The earthquake occurred in the middle of the S-net; therefore, the azimuthal coverage was very good. The IPFx and JMA EEW methods both provided sufficiently good performance, with a location error less than 15 km. The magnitude growth of the IPFx method is slightly faster than that of the JMA EEW method, and therefore, the warning threshold is exceeded earlier. Assuming no data transmission latency, the IPFx method can issue a public warning 5.7 s faster than the current EEW system.

Figure 9 shows the result of the earthquake that occurred at 9:35:54 on July 30, 2020. A false alarm was issued owing to the estimation of seismic intensity 5 upper even though no station recorded a seismic intensity of 1 or larger. This earthquake occurred near the Torishima island, and the station distribution was one-sided. The location error of the JMA EEW system was more than 400 km, and the magnitude was overestimated owing to the incorrect epicenter. Although the IPFx method did not use the island stations included in the JMA strong motion network, it could reduce the location error to only 31 km. Further, the estimated intensity error did not exceed the threshold for issuing a public warning.

Figure 10 shows the result of the earthquake that occurred at 11:02:26 on January 5, 2018, off Ibaraki prefecture. The JMA EEW system issued a false alarm because two earthquakes occurred within a few seconds of each other. Although the system detected two earthquakes, the magnitude was estimated from the amplitude caused by another earthquake. Therefore, the magnitude was overestimated and an inappropriate warning was issued. An offline simulation performed using the Hi-net data (because S-net was not available at the time) provided accurate estimates of the location and magnitude, and from the result, no public warnings would have been issued by the IPFx algorithm.

Discussion

Accuracy and Speed of the Source Estimation

The IPFx method detected all 129 earthquakes with observed seismic intensity $\geq$3. However, the July 5 event (M4.8) in the Northern Gifu prefecture had a large origin time error of 18 s. An active swarm related to volcanic activity occurred from April to July of 2020 at the boundary between the Nagano and the Gifu prefectures. Owing to this active seismicity, two M3 earthquakes occurred within 20 s before this event (see Figure 11). The first earthquake was detected by the IPFx method; however, the P-waves of the second and third earthquakes were not triggered owing to the coda waves of the first earthquake. Despite the large origin time error, the magnitude was appropriately estimated as 4.8, and the estimated seismic intensity was overestimated by just one unit.

The source estimation accuracy strongly depends on the station density and azimuthal coverage of the epicenter. The detection speed will improve if multiple networks are processed using a single method. The average P-wave detection and event detection speeds (excluding earthquakes on islands, where no seismic station is available for the IPFx method) became 1.9 s and 6.1 s faster than those of the JMA EEW method, respectively. Although the IPFx method needs more triggers than does the JMA EEW method, it offers improved event detection speed (Figure 7). The JMA EEW method uses an amplitude threshold to start the event detection process to avoid a noise trigger and wait for amplitude growth. Exceeding this threshold takes a long time — the order of tens of seconds when the magnitude is not very large. By contrast, the event detection criterion in the IPFx method, namely, three triggers in a trigger group of the mainland stations, helped speed-up the event detection and ensure accuracy.

The IPFx method is more sensitive than the JMA EEW method in that it detected all 129 earthquakes with seismic intensity $\geq$3, whereas the JMA EEW method missed 18 earthquakes. Although the sensitivity to small earthquakes may not be important from the viewpoint of issuing public warnings, it is essential for preventing false alarms. In this regard, one of the causes of the July 30 false alarm was the lack of enough triggers to locate the moderate earthquake precisely.

The possibility of false alarms with the IPFx method was evaluated. Eight earthquakes had maximum estimated seismic intensities $\geq$5 lower, and all were observed with seismic intensity $\geq$4. Therefore, all public warnings would have been accurate, whereas the JMA EEW method had one false alarm. Further, the IPFx method estimated 295 earthquakes with seismic intensities $\geq$3, but only 82 instances out of these did not exhibit seismic intensities $\geq$2 (71 for the JMA EEW method with the same criterion). Although these earthquakes are categorized as inaccurate estimates, the estimated location was very accurate, with an error $\leq$13 km for 95% of the earthquakes.

The IPFx method overestimated the seismic intensity for three reasons. First, the estimated magnitude of the earthquakes was larger than the observation. Specifically, because the magnitude equation used was tuned for relatively large earthquakes (M$\geq$5), the estimated magnitude tends to be overestimated relative to the catalog magnitude. This effect is especially significant for S-net, whose noise level is larger than that of inland stations. Second, the magnitude may be overwritten by a subsequent larger earthquake.

During active seismicity, multiple earthquakes occurred within a few tens of seconds. If a small earthquake precedes a large one, the IPFx method detects and locates the small one; however, its magnitude is overwritten by that of the large one because the process is active for at least 30 s (see Figure 11). Third, the observed intensities are recorded at seismic stations; however, the estimated intensity is computed at every site with a small grid spacing of 1 km. Therefore, the source-station distance tends to be short for the estimated seismic intensity, and it overestimates the observed intensity.

Real-time Testing Environment

The IPFx program was tested for 10 months continuously in a real-time environment. The waveform data are received as 1 s UDP packets at our server, and they are passed to the single-station processing as a standard input. The program is designed to handle packet loss (which initializes the recursive filter); however, disordered packets may cause problems in filtering. Future studies should aim to sort the sequence of the data before IPFx processing.

The station groups for the network processing (trigger group, estimation group, and cancellation group) are predefined based on the station configuration. The station groups are updated if the data are disconnected for a certain duration (in this study, 15 s) when no earthquake occurs. The disconnected station is removed and new station groups are computed. This process is repeated when the data are recovered.

To stabilize and speed-up the computation, the IPFx method was developed using the C++ language. A precomputed traveltime table was used to reduce the computation cost of the nonlinear process to obtain the waveform traveltime. The program can handle a dataset with around 1000 stations $\times$ 3 channels within the actual time. The single-station processing and network processing run in parallel, and the former usually takes more time.

To measure the computation time, the program was run in an offline environment. The computation time required for reading 1 h data from the hard disk and applying the IPFx method was 36 min (operation environment: CPU, Xeon 3.46 GHz; OS, Linux CentOS 6; memory, 48 GB; compiler, gcc ver.4.4.7). In other words, the average processing time for a 1 s packet is 0.6 s. Dividing the single-station processing across multiple cores can further reduce the processing time required in real applications.

The advantage of using continuous waveforms as input data is that the method can be directly applied to other seismic networks. Earthquake-prone countries have shown interest in the EEW system to mitigate seismic damage. Our proposed IPFx method has the potential to expand the JMA IPF method to global seismic networks.

Conclusion

This study developed the IPFx method by extending the IPF method used in the JMA EEW system. The proposed method uses continuous waveform data as an input instead of trigger information. In a 10-month continuous online test, this method performed better than the JMA EEW method in detecting earthquakes with a maximum seismic intensity $\geq$3 as per the JMA manual catalog. By merging multiple networks into a single method, both the P-wave detection and the event detection speeds were significantly improved compared to those of the current JMA EEW method. The two major false alarms on January 5, 2018, and July 30, 2020, were properly avoided by the IPFx method. The IPFx method provides an accurate shaking estimation even at the beginning of event detection, and it shows a seismic intensity error $<$0.2 at 5 s after event detection. The advantage of using continuous waveforms as input data is that this method can be applied to other seismic networks directly. Specifically, the IPFx method offers the potential of expanding the JMA IPF method to global seismic networks.

Data and Resources

We used the seismic waveform data in Hi-net (https://doi.org/10.17598/NIED.0003) and S-net (https://doi.org/10.17598/NIED.0007) (last accessed in November 2020), provided by National Research Institute for Earth Science and Disaster Resilience (NIED). There are one ssupplemental text explaining the detailed algorithm of network processing, one supplemental figure showing how the trigger information is processed to estimate source parameters in the network processing, and one supplemental table of the earthquake catalogs used in this study.

Acknowledgments

We thank the NIED for providing seismic waveform data. We thank Disaster Prevention Research Institute, Kyoto University for support the publication fee.

References

Allen, R. (1978). Automatic earthquake recognition and timing from single traces. *Bulletin of the Seismological Society of America*, 68(5):1521–1532.

Chung, A. I., Henson, I., and Allen, R. M. (2019). Optimizing earthquake early warning performance: Elarms-3. *Seismological Research Letters*, 90(2A):727–743.

Hamada, N. (1983). Improvement of the hypocenter determination program of the Japan meteorological agency (re-analyses of the hypocenter distribution of the 1980 earthquake swarm off the east coast of the Izu peninsula and the Matsushiro earthquake swarm). *Quart. J. Seism.*, 48:35–55. *(in Japanese with English abstract)*.

Hildyard, M. W., Nippress, S. E., and Rietbrock, A. (2008). Event detection and phase picking using a time-domain estimate of predominate period Tpd. *Bulletin of the Seismological Society of America*, 98(6):3025–3032.

Hildyard, M. W. and Rietbrock, A. (2010). Tpd, a damped predominant period function with improvements for magnitude estimation. *Bulletin of the Seismological Society of America*, 100(2):684–698.

Horiuchi, S., Negishi, H., Abe, K., Kamimura, A., and Fujinawa, Y. (2005). An automatic processing system for broadcasting earthquake alarms. *Bulletin of the Seismological Society of America*, 95(2):708–718.

Hoshiba, M. (2013). Real-time prediction of ground motion by Kirchhoff-Fresnel boundary integral equation method: Extended front detection method for earthquake early warning. *Journal of Geophysical Research: Solid Earth*, 118(3):1038–1050.

Hoshiba, M. and Aoki, S. (2015). Numerical shake prediction for earthquake early warning: Data assimilation, real-time shake mapping, and simulation of wave propagation. *Bulletin of the Seismological Society of America*, 105(3):1324–1338.

Kodera, Y., Hayashimoto, N., Moriwaki, K., Noguchi, K., Saito, J., Akutagawa, J., Adachi, S., Morimoto, M., Okamoto, K., and Honda, S. (2020). First-year performance of a nationwide earthquake early warning system using a wavefield-based ground-motion prediction algorithm in Japan. *Seismological Research Letters*, 91(2A):826–834.

Kodera, Y., Yamada, Y., Hirano, K., Tamaribuchi, K., Adachi, S., Hayashimoto, N., Morimoto, M., Nakamura, M., and Hoshiba, M. (2018). The propagation of local undamped motion (plum) method: A simple and robust seismic wavefield estimation approach for earthquake early warning. *Bulletin of the Seismological Society of America*, 108(2):983–1003.

Kuyuk, H. S., Allen, R. M., Brown, H., Hellweg, M., Henson, I., and Neuhauser, D. (2014). Designing a network-based earthquake early warning algorithm for california: Elarms-2. *Bulletin of the Seismological Society of America*, 104(1):162–173.

Liu, A. and Yamada, M. (2014). Bayesian approach for identification of multiple events in an early warning system. *Bulletin of the Seismological Society of America*, 104(3):1111–1121.

Tamaribuchi, K., Yamada, M., and Wu, S. (2014). A new approach to identify multiple concurrent events for improvement of earthquake early warning. *Zisin*, 67(2). *(in Japanese with English abstract).*

Ueno, H., Hatakeyama, S., Aketagawa, T., Funasaki, J., and Hamada, N. (2002). Improvement of hypocenter determination procedures in the Japan meteorological agency. *Quart. J. Seism.*, 65:123–134. *(in Japanese with English abstract).*

Urabe, T. (1991). Review: Transmission of Seismic Wave Data – Telemetry. *Zisin (Journal of the Seismological Society of Japan. 2nd ser.)*, 44(Supplement):15–26. *(in Japanese with English abstract).*

Urabe, T., Takano, K., Truruoka, H., and Nakagawa, S. (2013). Current status and next cloud computing of the Japan seismic observation data exchange and distribution network JDXnet. *IEICE technical report*, 113(256):21–23. *(in Japanese with English abstract).*

Wu, S., Yamada, M., Tamaribuchi, K., and Beck, J. (2014). Multi-events earthquake early warning algorithm using a Bayesian approach. *Geophysical Journal International*, 200(2):791–808.

Yamada, M., Tamaribuchi, K., and Wu, S. (2014). Faster and more accurate earthquake early warning system – combination of velocity and acceleration-type seismometers –. *J. Jpn. Assoc. Earthq. Eng.*, 14:21–34. *(in Japanese with English abstract).*

Zhu, L. (2003). Recovering permanent displacements from seismic records of the June 9, 1994 Bolivia deep earthquake. *Geophysical Research Letters*, 30(14).

Full mailing address for each author

1. Masumi Yamada: Disaster Prevention Research Institute, Kyoto University, Uji, Gokasho, 611-0011, Japan

2. Koji Tamaribuchi: Meteorological Research Institute, Tsukuba, 305-0052, Japan

3. Stephen Wu: The Institute of Statistical Mathematics, Tachikawa, 190-8562, Japan

List of Figure Captions

Figure 1. Flowchart of network processing step for processing data packet after single-station processing step. Here, S1-A1 corresponds to Stage 1: Action 1 in Figure S1.

Figure 2. Schematic diagram of station groups. Triangles indicate stations, and polygons show Voronoi cells. (a) Estimation group. (b) Trigger and cancellation groups.

Figure 3. Histograms of (a) location, (b) magnitude, and (c) seismic intensity errors for earthquakes with a seismic intensity $\geq$3. The JMA EEW and IPFx results compared to the JMA manual catalog are shown. The top-right numbers show the 95$^{\text{th}}$ percentile errors of earthquakes for the IPFx method compared to those from the JMA manual catalog.

Figure 4. Spatial distribution of (a) location, (b) magnitude, and (c) seismic intensity errors for earthquakes with seismic intensity $\geq$3.

Figure 5. Time history of (a) location, (b) magnitude, and (c) seismic intensity errors after event detection. Black and broken red lines respectively indicate the average errors for inland and offshore earthquakes. Gray and pink thin lines respectively indicate the error of individual events for inland and offshore earthquakes.

Figure 6. Histograms of earthquake magnitude for IPFx and JMA catalogs.

Figure 7. Time of first P-wave detection and first EEW report (event detection) for JMA EEW and IPFx method.

Figure 8. Result of earthquake on June 25, 2020. (a) Estimated source location at convergence time. Small and large stars, respectively, indicate the optimal estimation and the JMA manual catalog. Black and gray triangles respectively indicate triggered and nontriggered stations in the estimation group of this event. Open triangles indicate seismic stations. Colors indicate the particle weight. (b)–(d) Time history of estimated earthquake parameters after origin time. Thick and broken lines respectively indicate the result of the IPFx method and the JMA EEW

method. The circle at the right end shows the values in the JMA manual catalog. (b) location error, (c) magnitude error, and (d) seismic intensity error.

Figure 9. Result of earthquake on July 30, 2020. The format is the same as in Figure 8.

Figure 10. Result of earthquake on January 5, 2018. The format is the same as in Figure 8. The results of two different earthquakes are shown in (a).

Figure 11. Acceleration waveforms in vertical component as a function of epicenter distance for July 5 event (M4.8). The vertical line indicates the P-wave trigger. The gray lines indicate the P-wave onset for earthquakes with magnitude >3. The horizontal axis shows the time after 15:09:00.

Figures

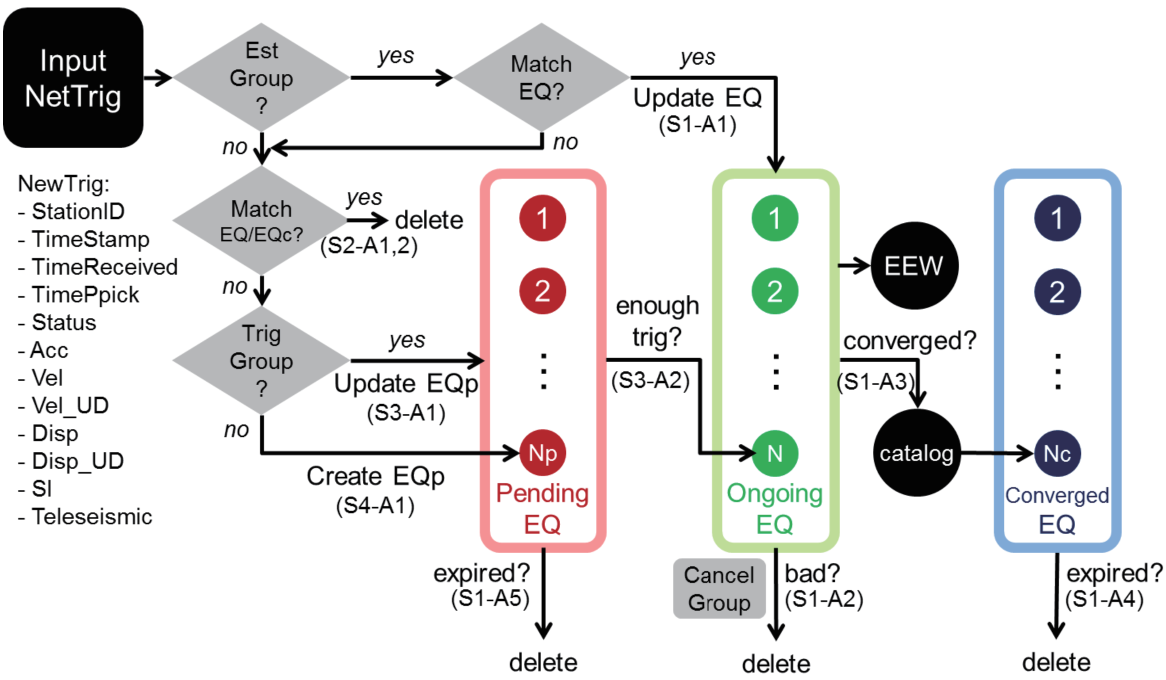

Figure 1. Flowchart of network processing step for a data packet after single-station processing step. Here, S1-A1 corresponds to Stage 1: Action 1 in Figure S1.

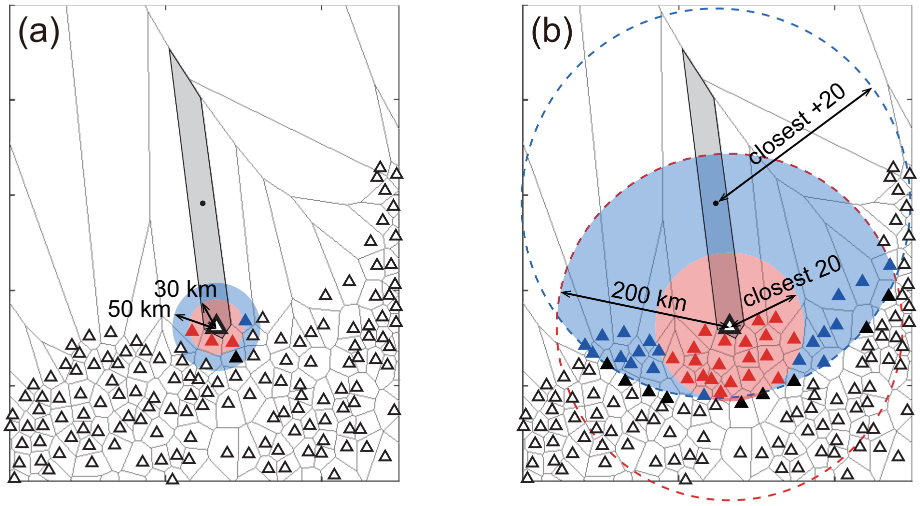

Figure 2. Schematic diagram of station groups. Triangles indicate stations, and polygons show Voronoi cells. (a) Estimation group. (b) Trigger and cancellation groups.

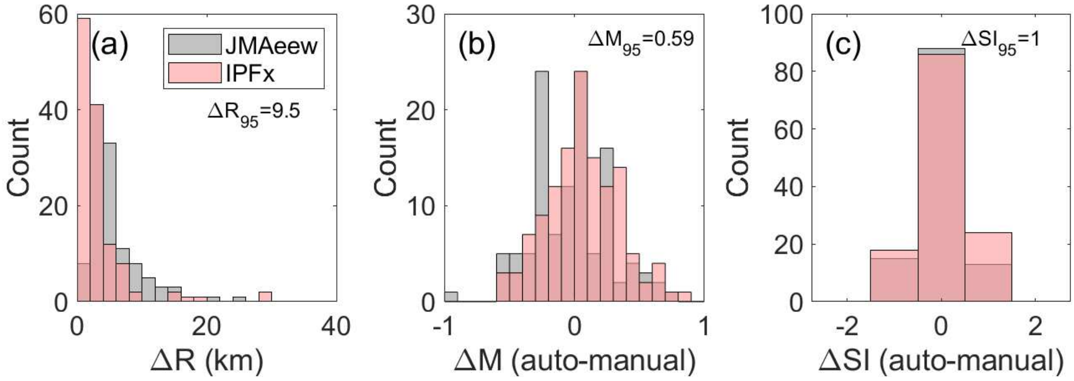

Figure 3. Histograms of (a) location, (b) magnitude, and (c) seismic intensity errors for earthquakes with a seismic intensity ≥3. The JMA EEW and IPFx results compared to the JMA manual catalog are shown. The top-right numbers show the 95^{th} percentile errors of earthquakes for the IPFx method compared to those from the JMA manual catalog.

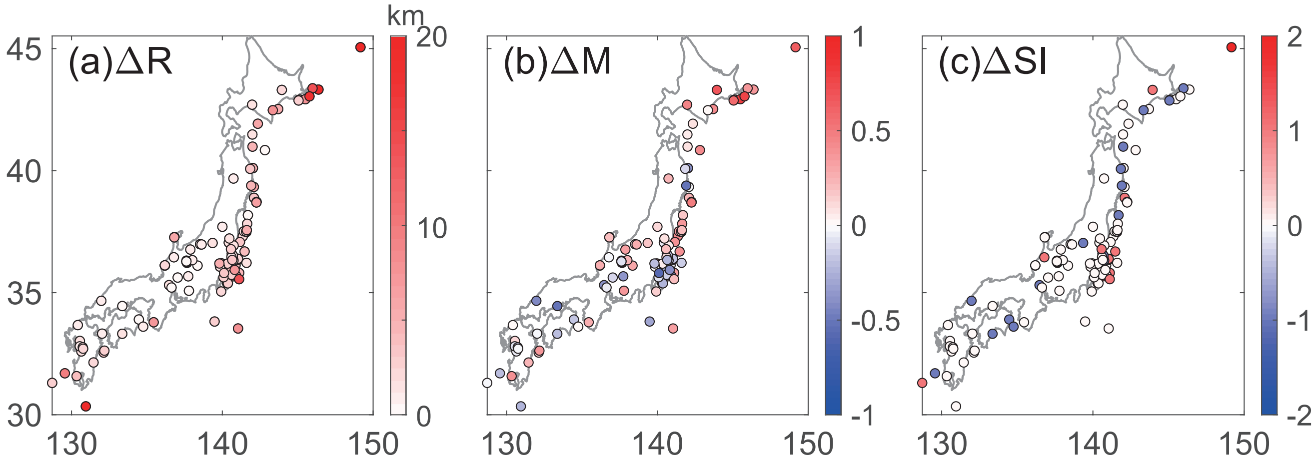

Figure 4. Spatial distribution of (a) location, (b) magnitude, and (c) seismic intensity errors for earthquakes with seismic intensity ≥3.

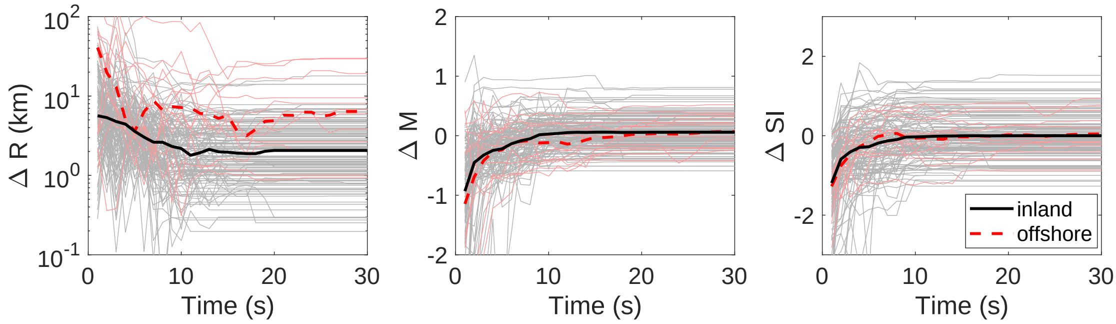

Figure 5. Time history of (a) location, (b) magnitude, and (c) seismic intensity errors after event detection. Black and broken red lines respectively indicate the average errors for inland and offshore earthquakes. Gray and pink thin lines respectively indicate the error of individual events for inland and offshore earthquakes.

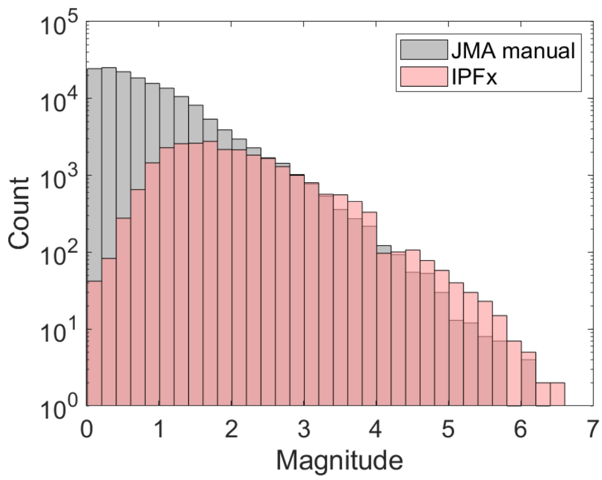

Figure 6. Histograms of earthquake magnitude for IPFx and JMA catalogs.

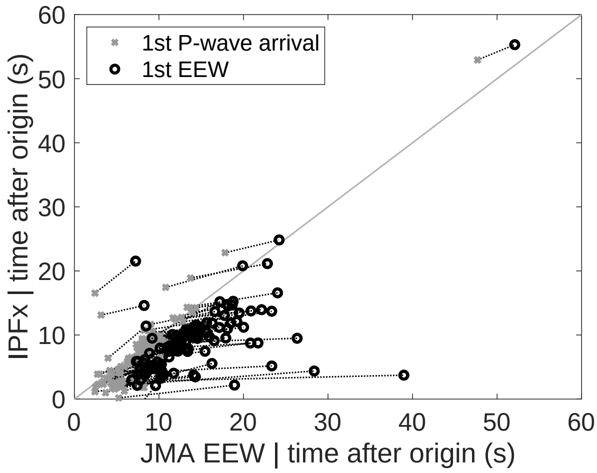

Figure 7. Time of first P-wave detection and first EEW report (event detection) for JMA EEW and IPFx method.

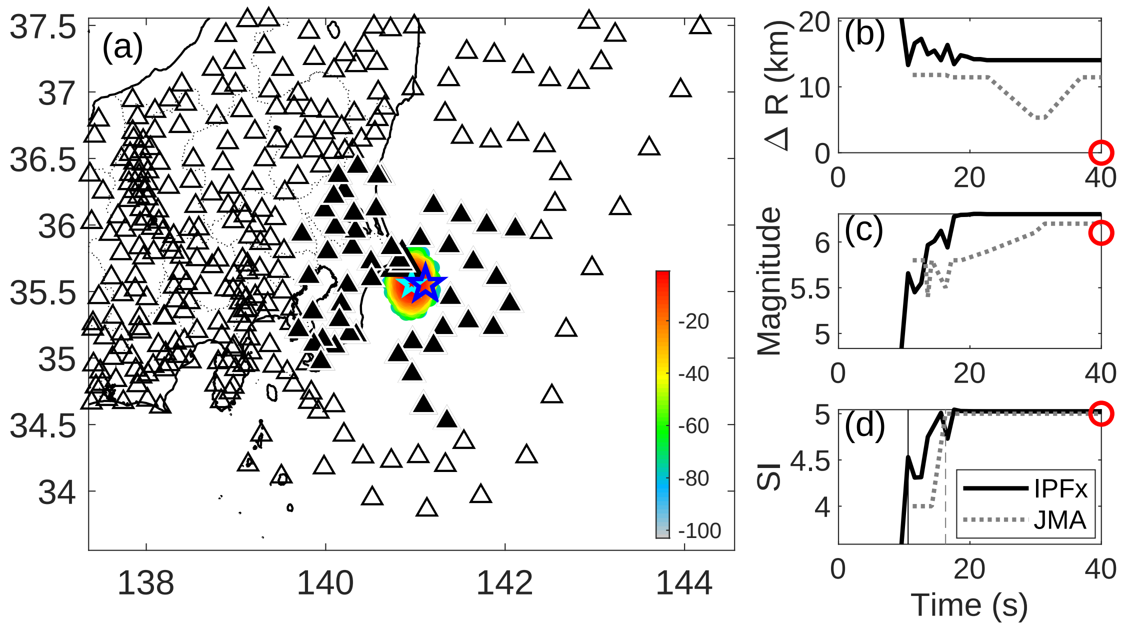

Figure 8. Result of earthquake on June 25, 2020. (a) Estimated source location at convergence time. Small and large stars, respectively, indicate the optimal estimation and the JMA manual catalog. Black and gray triangles respectively indicate triggered and nontriggered stations in the estimation group of this event. Open triangles indicate seismic stations. Colors indicate the particle weight. (b)–(d) Time history of estimated earthquake parameters after origin time. Thick and broken lines respectively indicate the result of the IPFx method and the JMA EEW method. The circle at the right end shows the values in the JMA manual catalog. (b) location error, (c) magnitude error, and (d) seismic intensity error.

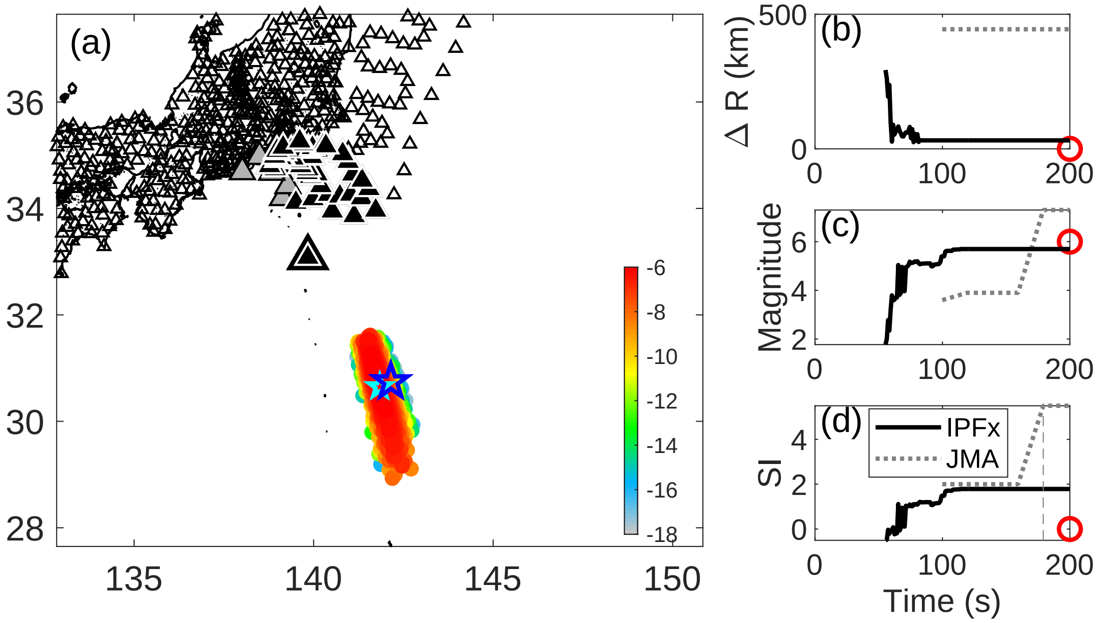

Figure 9. Result of earthquake on July 30, 2020. The format is the same as in Figure 8.

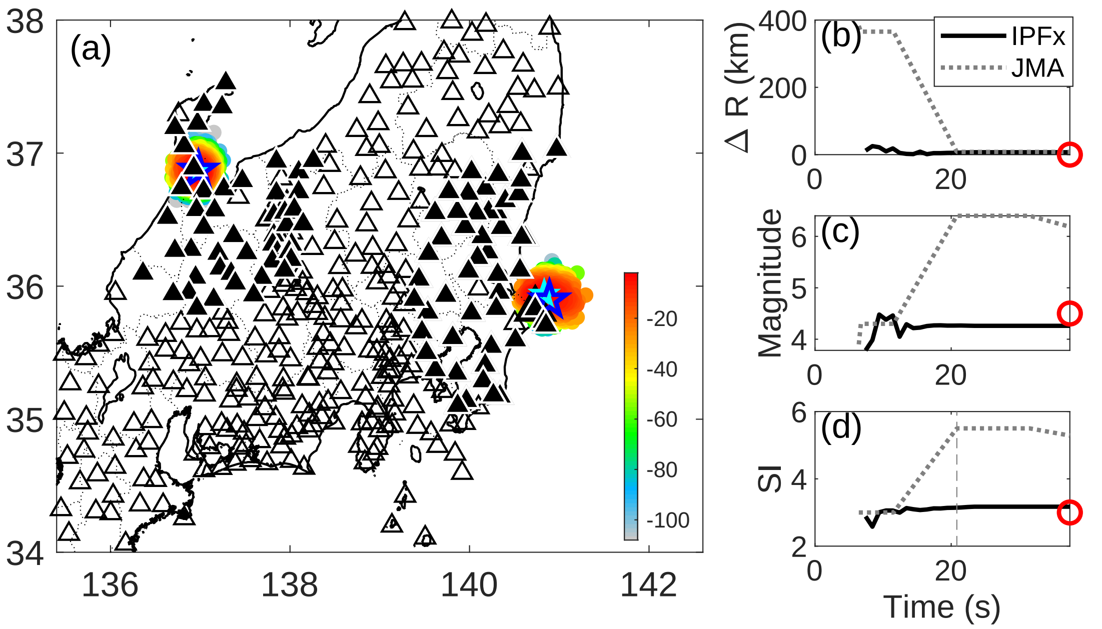

Figure 10. Result of earthquake on January 5, 2018. The format is the same as in Figure 8.

The results of two different earthquakes are shown in (a).

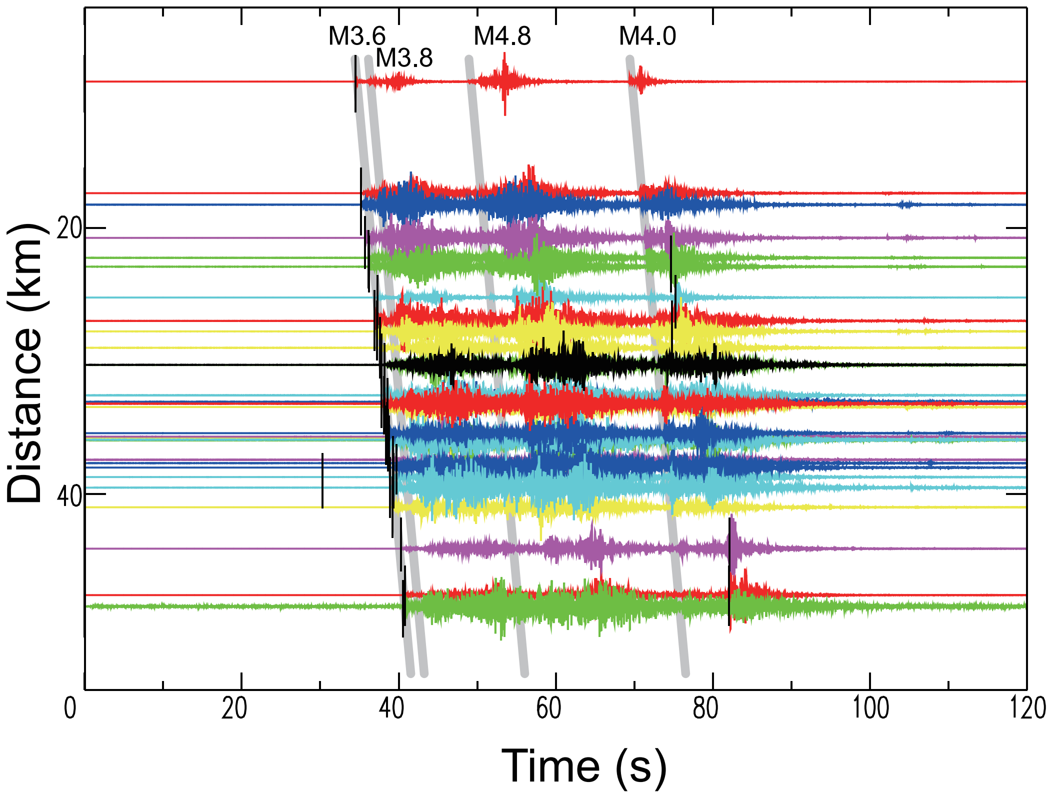

Figure 11. Acceleration waveforms in vertical component as a function of epicenter distance for July 5 event (M4.8). The vertical line indicates the P-wave trigger. The gray lines indicate the P-wave onset for earthquakes with magnitude >3. The horizontal axis shows the time after 15:09:00.